The kinetic rate of micropore collapse in compact amorphous solid water

Catherine R. Hill* and Helen J. Fraser
The Open University, Department of Physical Sciences, Walton Hall, Milton Keynes, MK7 6AA, UK

Thomas Loerting
Institute of Physical Chemistry, University of Innsbruck, Innrain 52a, A-6020 Innsbruck, Austria

Tristan G. A. Youngs and Daniel T. Bowron
ISIS Facility, Rutherford Appleton Laboratory, Harwell Oxford, Didcot, Oxon, OX11 0QX, UK
(Dated: September 12, 2014)

INTRODUCTION

Amorphous solid water (ASW) is one of multiple solid phases of water ice; a group which includes both crystalline and amorphous forms. It is thought to be the most common form of ice found in the universe, situated on interstellar dust grains [1], on comets [2–5] and planetary satellites [6], and it is thought that is may play a role in planet formation [7]. ASW is distinct from other forms of amorphous ice. These other forms include low density, high density and very high density amorphous ice (formed by compressing hexagonal crystalline ice) and hyperquenched glassy water, which is formed by rapid quenching of micron sized water droplets [7]. It undergoes a phase change to cubic crystalline ice via a glass transition at around 137 K [8, 9].

In space, ASW can form by grain surface reactions [10–12]; it is also possible that it can form by vapour deposition through sputtering of water from shocks and outflows or in dark clouds [13, 14]. In the laboratory, it is always formed by vapour deposition; at low temperatures (around 10 K) this produces a very porous ASW [15, 16] which undergoes a phase change to a more compact ASW between 38 and 68 K [17–19]. The more compact form of ASW still displays significant microporosity [18–20]. The results of numerous experiments investigating the porosity of ASW by studying dangling OH bonds [21–23], gas adsorption [18, 24–28] and desorption [29, 30] or positron spectroscopy [31, 32] show that the pores collapse on heating. A small angle neutron scattering study by Mitterdorfer *et al.* [33] investigated for the first time the nature of the pore collapse and shape of the pores, finding that the pores collapse from cylinders to platelets between 120 and 140 K, depending on the method of deposition. This work builds on that study, investigating for the first time the kinetic rate of pore collapse and the precise temperature at which this happens.

EXPERIMENTAL METHODS

The pore collapse of ASW was studied by neutron scattering, a non destructive method for probing the structure of a material. Studying the pore collapse of ASW using neutron scattering presents something of a challenge; changes related to crystallisation are seen in the large angle scattering (Q >1 $Å^{-1}$) whereas changes related to the pores are seen in the small angle region (Q <1 $Å^{-1}$). NIMROD (the Near and InterMediate Range Order Diffractometer) of the ISIS second target station is a unique instrument that allows measurements to be taken on a continuous length scale from <1 - 300 $Å^{-1}$ in a single measurement [34], allowing simultaneous detection of crystallisation and pore collapse.

The ASW sample used in this study was produced by vapour deposition using the method described in reference [35]. D_2O vapour was deposited via background deposition on a copper plate cooled to 77 K with liquid nitrogen at a growth rate of around 40 μm per hour. This is achieved with a background pressure of 1×10^{-4} mbar and a water pressure of 0.1 mbar. The flow rate is controlled with a needle valve next to the D_2O reservoir. After a deposition time of between 24 and 30 hours, the ASW was scraped off the copper plate under liquid nitrogen, stored under liquid nitrogen and shipped to ISIS. Once at ISIS, the sample was transferred under liquid nitrogen to a TiZr null scattering cell which was placed in a helium cryostat, maintaining the sample temperature of 77 K. The cryostat was then placed on the beamline and measurements were taken as follows. The cryostat was first held at 80 K while neutron scattering data was collected. Data was taken while heating to 95 K at a rate of 0.3 K per minute. The cryostat was then held at 95 K and the process repeated for 125 K, 137 K and 144 K. This led to the collection of data at sample temperatures of 92 K, 117 K, 136 K and 144 K with heating data taken in between these regions.

RESULTS AND DISCUSSION

Fig. 1a. shows the neutron scattering patterns obtained for heating the sample between 78 and 144 K. The low Q region (Q <1 $Å^{-1}$) features a slope with a hump superimposed upon it at around 0.1 $Å^{-1}$. The slope is indicative of a granular material and is due to scattering

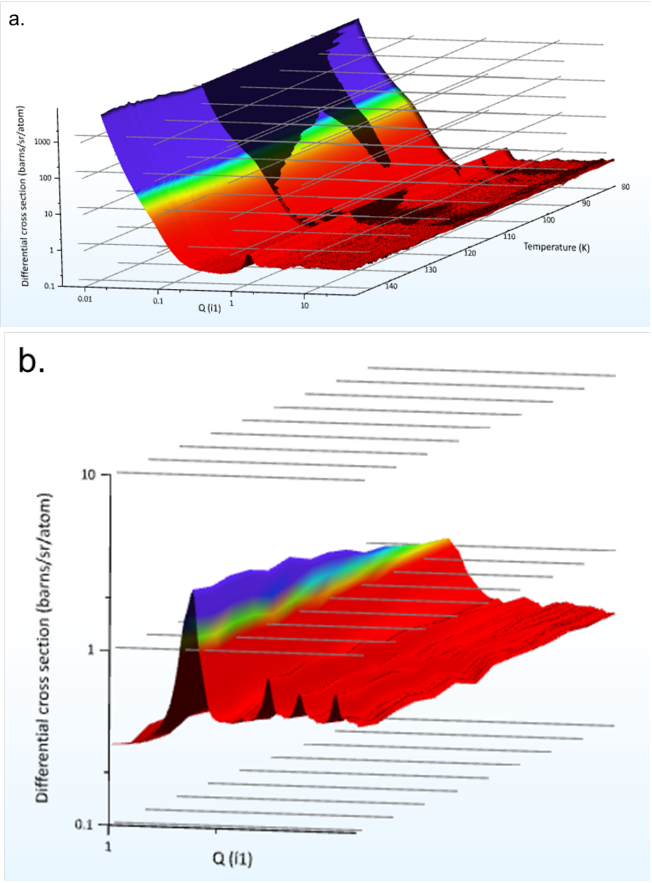

FIG. 1. **a.** Neutron scattering patterns for the entire heating data set between 78 and 144 K. The hump at around 0.1 Å^{-1} is indicative of a porous media and its flattening with temperature shows of pore collapse. The high Q region (Q >1 Å^{-1}) contains no Bragg peaks which would indicate crystallisation, showing that the pore collapse is unrelated to crystallisation. **b.** High Q data obtained when keeping the sample temperature at 144 K. The three Bragg peaks that appear indicate crystallisation to cubic crystalline ice.

from the surfaces of the grains. In the very low Q region (Q <0.05 Å^{-1}), the slope can be fitted by a Porod function ($y = ax^{-b}$), giving an exponent (b) between 4.01 and 5.61. The hump flattens between 117 and 136 K; such a flattening of this hump has been found to be indicative of pore collapse [33]. The lack of Bragg peaks in the high Q region (Q >1 Å^{-1}) demonstrates that the pore collapse is not related to crystallisation to cubic crystalline ice (I_c). Crystallisation only occurs when holding the sample at 144 K (Fig. 1b.). In order to investigate the nature of the pore collapse, two approaches were taken to analyse the low Q data. The first is to extract the specific surface area using the method proposed by Paglia *et al.* [36], and the second is to use the "new Guinier-Porod model" developed by Hammouda *et al.* [37].

The specific surface area is calculated as follows. Paglia *et al.* state that the Porod constant can be found from the intercept of the quasi-plateau of an $I(Q).Q^4$ plot:

$$\Sigma_s = \frac{1}{\rho_m}.\frac{\lim_{Q\to\infty}(I(Q).Q^4)}{2\pi\Delta\rho^2} = \frac{1}{\rho_m}.\frac{K}{2\pi\Delta\rho^2} \qquad (1)$$

The calculated specific surface areas are shown in Fig. 2 versus time. The temperature regions are indicated on the graph. The larger errors at lower temperatures are due to the lack of a flat plateau in the $I(Q).Q^4$ plots; in these cases, the midpoint of the linear region was chosen and the error bars indicate the start and end of the linear region. Once the quasi-plateau appears, the errors become a lot smaller as the y intercepts of the start and end of the plateau are now very close together. The specific surface area is around 150 m^2 cm^{-3} at the start and increases to around 200 m^2 cm^{-3} between 92 and 117 K. This is thought to be due to restructuring below the glass transition temperature and a more detailed analysis of this will be published elsewhere. Between 117 K and 136 K, the specific surface area decreases rapidly to around 50 m^2 cm^{-3} which is indicative of pore collapse. The collapse continues at a slower rate while the sample is held at 136 K and also when heating to 144 K. By 144 K, the specific surface area has reached its minimum at around 40 m^2 cm^{-3}. It can be seen that the specific surface area remains constant when the temperature is held constant (at 92 K and 117 K) as long as the temperature is below the glass transition temperature (around 137 K [8, 9]). This indicates that restructuring of the ice (including pore collapse) is not an auto catalytic process below the glass transition temperature; it requires an input of energy in order to progress.

The "new Guinier-Porod model" [37] is an alternative to the standard Guinier and Porod fits and takes into account varying pore shapes. Instead of dividing the data into regions and fitting a Guinier or a Porod function to each region, the following model is fitted between around 0.045 and 0.2 Å^{-1} (exact ranges depend on the shape of the data at each temperature):

$$I(Q) = \frac{G}{Q^s} exp(\frac{-Q^2 {R_g}^2}{3-s}) \text{ for } Q \le Q_1$$
$$I(Q) = \frac{D}{Q^d} \text{ for } Q \ge Q_1 \qquad (2)$$
$$Q_1 = \frac{1}{R_g}\left[\frac{(d-s)(3-s)}{2}\right]^{1/2}$$

The parameters R_g and s are of particular interest. R_g is the radius of gyration of the pores, giving an indication of their size. s is a dimensionality parameter giving information on the shape of the pores. A value of 0 indicates spheres, a value of 1 indicates cylinders and a value of 2 indicates platelets. It can be seen from a consideration of equation 2 that as s approaches 3, the size of the pores tends to zero.

Fig. 3 shows the values of R_g and s versus time, with temperature regions indicated on the graph. At the start,

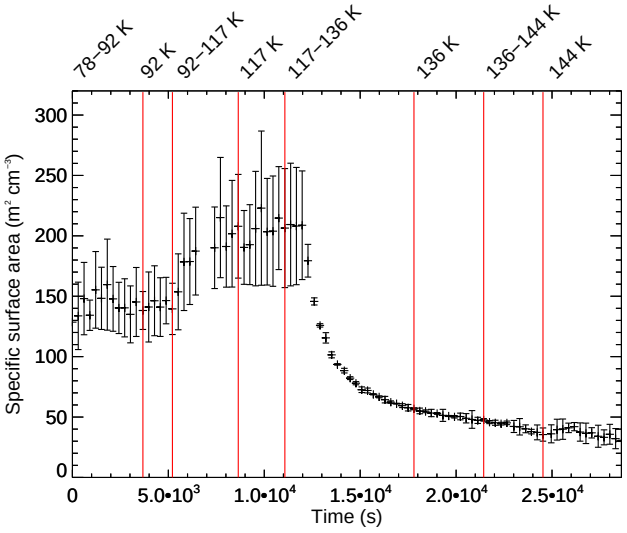

FIG. 2. Specific surface area values calculated from Porod constants extracted from the quasi-plateaus of $I(Q).Q^4$ plots. Where quasi-plateaus were not present, the Porod constant was taken as the midpoint of the linear regime and the errors were extracted from the start and end of this region. Elsewhere, the errors represent the start and end points of the plateau intercepts.

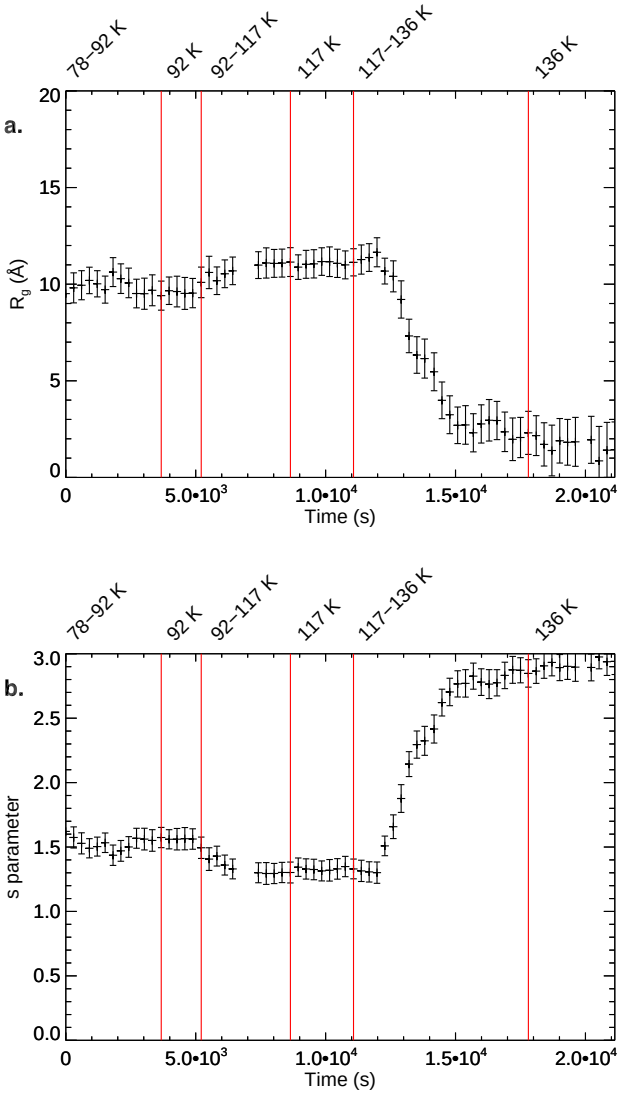

FIG. 3. **a.** Extracted radius of gyration (R_g) of the pores versus time. **b.** Extracted s parameter for the pores versus time. s is a dimensionality parameter; a value of 1 indicates cylinders, a value of 2 indicates platelets and a value close to 3 represents total pore collapse. There is some restructuring of the pores between 92 and 117 K and a clear collapse from cylinders to platelets between 117 and 136 K.

R_g is around 10 Å and s is around 1.5, indicating cylindrical pores. Between 92 and 117 K, R_g increases to around 11 Å and s decreases to around 1.3 which is indicative of a slight elongation of the pores. As mentioned previously, this restructuring will be the subject of another publication. Again, when the sample is held at 92 and 117 K, there is no change to either parameter, indicating that changes to the pores are not auto catalytic. It is clear from these graphs that the pore collapse begins between 117 and 136 K, with a decrease of R_g to around 2.5 Å and an increase of s to around 2.8. The pores appear to have fully collapsed by this point as the values of R_g and s remain constant in the isothermal at 136 K region. It should be noted that the Guinier-Porod model only provides a good fit when the ice is sufficiently porous, hence the lack of data beyond 136 K.

In order to extract the temperature of the onset of pore collapse and the rate of the collapse, the specific surface area and Guinier-Porod data were plotted against temperature between 117 and 136 K (Fig. 4). Both models provide a consistent picture: the pore collapse starts at 121 K. The red line on the R_g plot (Fig. 4.b.) shows an exponential fit to the data which gives the rate equation for the radius of gyration:

$$R_g = -0.00554exp(0.05909T) + 18.88424 \qquad (3)$$

It should be noted that this rate equation is likely to be highly specific to the ice sample and the conditions under which it was produced. It has already been shown that the temperature of pore collapse depends on the deposition conditions [33], with collapse taking place at a higher temperature for samples grown with a non baffled flow than for samples grown with a baffled flow (as was the one in the present study). The growth temperature also affects porosity [17–19] and is therefore likely to affect the temperature of collapse and the rate of collapse. It is also possible that the thermal history of the material may affect the pore collapse. Further work is clearly needed to investigate what effects (if any) these factors have on the rate of pore collapse. However, this result is valuable as an indication of the rate of pore collapse

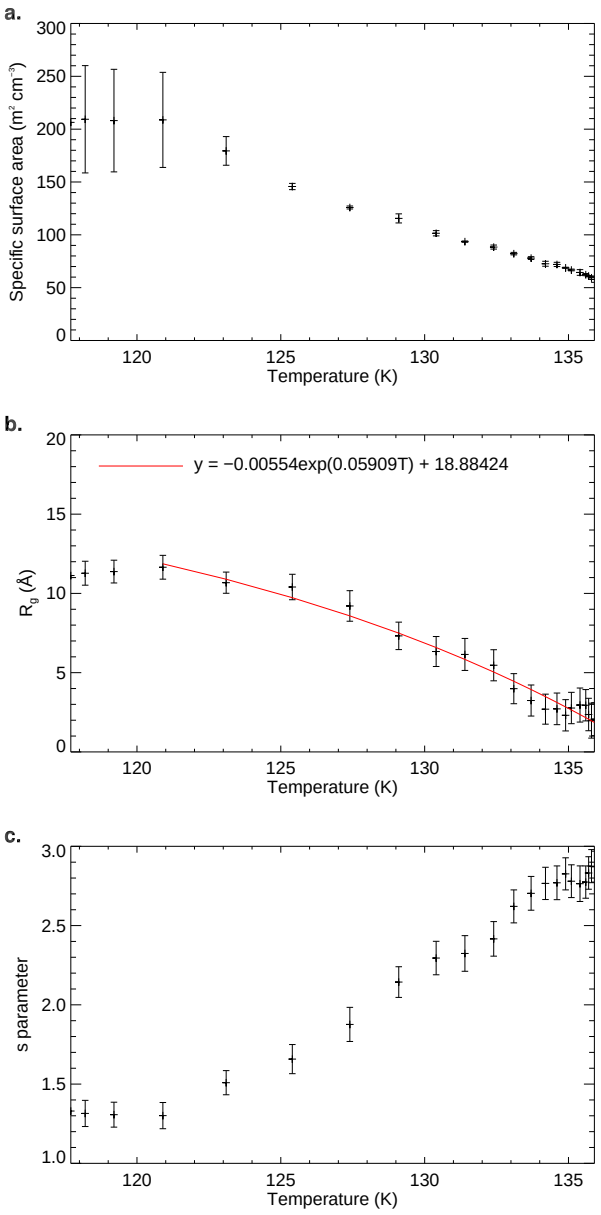

FIG. 4. **a.**Reduction in specific surface area versus temperature between 117 and 136 K. **b.** Reduction of radius of gyration (R_g) between 117 and 136 K. The rate equation for this reduction is shown in red. **c.** Increase in s parameter from 1 to nearly 3 between 117 and 136 K, indicating a collapse from cylinders to platelets.

in a sample of this type (baffled flow of 40 μm per hour grown at 77 K).

* catherine.hill@open.ac.uk

[1] A. Leger, J. Klein, S. D. Cheveigne, C. Guinet, D. Defourneau, and M. Belin, A&A **79**, 256 (1979).

[2] H. Patashni, G. Rupprech, and D. W. Schuerma, Nature **250**, 313 (1974).

[3] J. Klinger, Icarus **47**, 320 (1981).

[4] R. Smoluchowski, Ap. J. **244**, L31 (1981).

[5] A. H. Delsemme, Journal of Physical Chemistry **87**, 4214 (1983).

[6] R. Smoluchowski, Science **201**, 809 (1978).

[7] P. Ehrenfreund, H. J. Fraser, J. Blum, J. H. E. Cartwright, J. M. Garcia-Ruiz, E. Hadamcik, A. C. Levasseur-Regourd, S. Price, F. Prodi, and A. Sarkissian, Planetary and Space Science **51**, 473 (2003).

[8] R. S. Smith, C. Huang, and B. D. Kay, Journal of Physical Chemistry B **101**, 6123 (1997).

[9] R. S. Smith and B. D. Kay, Nature **398**, 788 (1999).

[10] S. Ioppolo, H. M. Cuppen, C. Romanzin, E. F. van Dishoeck, and H. Linnartz, Ap. J. **686**, 1474 (2008).

[11] Y. Oba, N. Miyauchi, H. Hidaka, T. Chigai, N. Watanabe, and A. Kouchi, Ap. J. **701**, 464 (2009).

[12] H. M. Cuppen, S. Ioppolo, C. Romanzin, and H. Linnartz, PCCP **12**, 12077 (2010).

[13] D. A. Williams, T. W. Hartquist, and D. C. B. Whittet, MNRAS **258**, 599 (1992).

[14] R. Papoular, MNRAS **362**, 489 (2005).

[15] K. P. Stevenson, G. A. Kimmel, Z. Dohnalek, R. S. Smith, and B. D. Kay, Science **283**, 1505 (1999).

[16] G. A. Kimmel, K. P. Stevenson, Z. Dohnalek, R. S. Smith, and B. D. Kay, Journal of Chemical Physics **114**, 5284 (2001).

[17] P. Jenniskens, D. F. Blake, M. A. Wilson, and A. Pohorille, Ap. J. **455**, 389 (1995).

[18] N. Horimoto, H. S. Kato, and M. Kawai, Journal of Chemical Physics **116**, 4375 (2002).

[19] M. P. Collings, J. W. Dever, H. J. Fraser, M. R. S. McCoustra, and D. A. Williams, Ap. J. **583**, 1058 (2003).

[20] K. Isokoski, J. B. Bossa, T. Triemstra, and H. Linnartz, PCCP **16**, 3456 (2014).

[21] V. Buch and J. P. Devlin, Journal of Chemical Physics **94**, 4091 (1991).

[22] M. A. Zondlo, T. B. Onasch, M. S. Warshawsky, M. A. Tolbert, G. Mallick, P. Arentz, and M. S. Robinson, Journal of Physical Chemistry B **101**, 10887 (1997).

[23] L. Schriver-Mazzuoli, A. Schriver, and A. Hallou, Journal of Molecular Structure **554**, 289 (2000).

[24] R. Pletzer and E. Mayer, Journal of Chemical Physics **90**, 5207 (1989).

[25] P. Ayotte, R. S. Smith, K. P. Stevenson, Z. Dohnalek, G. A. Kimmel, and B. D. Kay, Journal of Geophysical Research-Planets **106**, 33387 (2001).

[26] C. S. Boxe, B. R. Bodsgard, W. Smythe, and M. T. Leu, Journal of Colloid and Interface Science **309**, 412 (2007).

[27] U. Raut, M. Famá, B. D. Teolis, and R. A. Baragiola, Journal of Chemical Physics **127** (2007).

[28] O. Gálvez, B. Maté, V. J. Herrero, and R. Escribano, Icarus **197**, 599 (2008).

[29] M. T. Sieger and T. M. Orlando, Surface Science **451**, 97 (2000).

[30] L. Hornekaer, A. Baurichter, V. V. Petrunin, A. C. Luntz, B. D. Kay, and A. Al-Halabi, Journal of Chemical Physics **122** (2005).

[31] Y. C. Wu, A. Kallis, J. Jiang, and P. G. Coleman, Physical Review Letters **105** (2010).

[32] Y. C. Wu, J. Jiang, S. J. Wang, A. Kallis, and P. G. Coleman, Physical Review B **84** (2011).

[33] C. Mitterdorfer, M. Bauer, T. G. A. Youngs, D. T.

Bowron, J. L. Finney, C. R. Hill, H. J. Fraser, and T. Loerting, PCCP (2014).
[34] D. T. Bowron, A. K. Soper, K. Jones, S. Ansell, S. Birch, J. Norris, L. Perrott, D. Riedel, N. J. Rhodes, S. R. Wakefield, A. Botti, M. A. Ricci, F. Grazzi, and M. Zoppi, Review of Scientific Instruments **81** (2010).
[35] E. Mayer and R. Pletzer, Journal of Chemical Physics **80**, 2939 (1984).
[36] G. Paglia, C. E. Buckley, T. J. Udovic, A. L. Rohl, F. Jones, C. F. Maitland, and J. Connolly, Chemistry of Materials **16**, 1914 (2004).
[37] B. Hammouda, Journal of Applied Crystallography **43**, 716 (2010).